Interpreting magnetic fabrics in amphibole-bearing rocks

Andrea R. Biedermann[a,b], Karsten Kunze[c], Ann M. Hirt[a]

[a] Institute of Geophysics, ETH Zurich, Sonneggstrasse 5, 8092 Zurich, Switzerland

[b] Institute for Rock Magnetism, University of Minnesota, 116 Church St SE, 55455 Minneapolis, United States of America

[c] Scientific Centre for Optical and Electron Microscopy, ETH Zurich, Auguste-Piccard-Hof 1, 8093 Zurich, Switzerland

Corresponding author

Andrea R. Biedermann
237 John T. Tate Hall
Institute for Rock Magnetism
University of Minnesota
116 Church St SE
Minneapolis, MN 55455
United States of America

andrea.regina.biedermann@gmail.com
+1 612 434 66 60

The final version of this article is available on the Tectonophysics website

Abstract
If amphibole is a major constituent in a rock, its magnetic fabric can be largely controlled by the crystallographic preferred orientation of amphibole. This study describes the (para-)magnetic anisotropy in two amphibolites, both containing ca. 70 % hornblende with rather strong crystallographic preferred orientation. Both amphibolites display a significant and well-defined anisotropy of magnetic susceptibility, with the minimum susceptibility approximately normal to foliation. However, in one amphibolite, the maximum susceptibility is parallel to the lineation, whereas in the other it is not. This seemingly inconsistent observation can be explained by the intrinsic susceptibility anisotropy of single crystals of hornblende, and their texture in the rocks. Numerical models show how the principal susceptibility axes relate to macroscopic foliation and lineation for point and fiber textures. This study underlines the potential of using magnetic anisotropy to obtain information about mineral fabrics in mafic rocks. At the same time, it highlights the necessity for taking into account single crystal properties of the mineral(s) responsible for the anisotropy and their crystallographic preferred orientation when interpreting magnetic fabrics.

Highlights

- AMS modeled from amphibole CPO and single crystal susceptibility tensor

- Minimum susceptibility normal to foliation

- Magnetic and mineral lineation coaxial if c-fiber texture

- Maximum susceptibility varies up to 90° to lineation for point or a-fiber texture

Keywords: Amphibolite, hornblende, magnetic fabric, AMS, crystallographic preferred orientation, CPO, EBSD, texture, mineral fabric

1. Introduction
Mineral fabrics can provide important information about the geological and geodynamic processes that a rock has experienced over its history, such as flow, deformation or recrystallization in a stress field. The mineral fabric is a complex property of a rock, which involves crystallographic preferred orientation (CPO), shape preferred orientation (SPO), and spatial distribution of various minerals, defects, or other fabric indicators. Macroscopic foliation and lineation are defined by the (shape) preferred orientation and alignment of platy and elongated minerals, respectively. Textures, here used synonymously to CPO, can be quantified by techniques such as electron backscatter diffraction (EBSD), X-ray texture goniometry, or neutron diffraction.

Many physical properties of minerals, e.g. elastic, thermal, or magnetic properties of single crystals, are intrinsically anisotropic. Therefore, the anisotropy of physical properties of a rock is linked to the CPO and/or SPO of its constituent minerals, and thus provides an indirect measure of mineral fabrics. Texture, in turn, can be used to infer the geodynamic context of the rock. The attraction in using physical properties as an indirect measure of texture is that they are faster than direct texture determination, and can be performed on larger samples that are more representative of heterogeneous materials (Engler and Randle, 2009; Ullemeyer et al., 2000). The relationship between anisotropy of tensorial properties and texture has long been established (e.g. Bunge, 1969, 1982; Ji and Mainprice, 1989; Mainprice and Nicolas, 1989; Seront et al., 1993). Mathematical models allow to compute the anisotropy of elastic or other physical properties of a rock based on its texture (Mainprice, 1990; Mainprice and Humbert, 1994; Mainprice et al., 2011; Wenk et al., 1998). These models have been used to (1) model elastic or thermal tensors and compare them to measured anisotropy, or (2) to predict or extrapolate seismic anisotropy when it was not directly measured (Brownlee et al., 2011, 2013; Feinberg et al., 2006; Lloyd et al., 2011; Tommasi et al., 2001). Even though the same approach can be applied to magnetic fabrics, the newest studies comparing rock texture with magnetic and seismic anisotropies show texture-derived models only for seismic, but not for magnetic anisotropy (e.g. Gaudreau et al., 2017; Punturo et al., 2017).

Anisotropy of magnetic susceptibility (AMS), specifically the degree of anisotropy and orientation of principal susceptibility axes, is commonly used as a qualitative indicator for mineral fabrics (e.g. Borradaile and Henry, 1997; Borradaile and Jackson, 2010; Hrouda, 1982; Martín-Hernández et al., 2004; Owens and Bamford, 1976; Tarling and Hrouda, 1993, and references therein). The maximum susceptibility (k_1 or magnetic lineation) is typically parallel to lineation, and the minimum susceptibility (k_3, or pole to magnetic foliation) normal to the foliation plane (Balsley and Buddington, 1960). Numerous studies report that the degree of magnetic anisotropy increases with progressive deformation (e.g. Cogné and Perroud, 1988; Graham, 1966; Hirt et al., 1988; Kligfield et al., 1977; Kneen, 1976; Rathore, 1979; Wood et al., 1976). However, these empirical relationships are further influenced by mineralogy (Borradaile and Henry, 1997; Owens, 1974). It was also confirmed that AMS, when carried by a single mineral, reflects the CPO of that same mineral (Chadima et al., 2004; Hirt et al., 1995; Hrouda et al., 1985; Hrouda et al., 1997; Hrouda and Schulmann, 1990; Kligfield et al., 1983; Lüneburg et al., 1999; Owens and Rutter, 1978; Siegesmund et al., 1995). For rocks with more complex fabrics, and several minerals potentially contributing to AMS, EBSD has been used to determine which minerals carry the AMS (e.g. Bascou et al., 2002; 2013; Boiron et al., 2013; Cavalcante et al., 2013; Chadima et al., 2009; Craddock and McKiernan, 2007; Kruckenberg et al., 2010; Oliva-Urcia et al., 2012; Viegas et al., 2013; Zak et al., 2008). Results from these investigations illustrate that prior to interpreting magnetic fabrics, it is important to (1) determine which mineral carries the AMS, and (2) know the single-crystal AMS of this mineral and its variation with chemical composition. Advanced measurement techniques that isolate individual components of the AMS (e.g. Martin-Hernandez and Ferré, 2007), combined with knowledge about the single crystal properties, now allow for a more precise, quantitative interpretation of magnetic fabrics, similar to what is already being done in seismic anisotropy studies.

One further challenge in interpreting magnetic fabrics is observed in amphibole-bearing rocks, where magnetic lineation is an unreliable proxy for the macroscopic lineation. Amphiboles occur in a wide range of igneous and metamorphic rocks, and possess a long prismatic habit as well as crystal plastic anisotropy, so they often adopt a CPO during deformation or flow. Together with phyllosilicates, amphiboles are among the most important carriers of (para)magnetic fabrics in various igneous and metamorphic rock types (Borradaile et al., 1993; Schulmann and Ježek, 2011; Zak et al., 2008). Although the maximum susceptibility (k_1) in amphibole-bearing rocks can reflect the macroscopic foliation and lineation, Borradaile et al. (1993) observed some ‘anomalous fabrics’; rocks in which k_1 lies in the foliation plane, but perpendicular to the macroscopic lineation. Similarly, amphibolites in the Møre-Trøndelag Fault Zone, Central Norway, show maximum susceptibility axes deviating up to 50° from the structural lineation (Biedermann, 2010).

Early studies on the intrinsic AMS of amphibole single crystals reported differing and partly conflicting results, which were attributed to the presence of ferromagnetic inclusions (Borradaile et al., 1987; Finke, 1909; Lagroix and Borradaile, 2000; Parry, 1971; Wagner et al., 1981). Recently, Biedermann et al. (2015a) characterized the isolated paramagnetic AMS in amphibole minerals of well-defined composition. In hornblende and actinolite, they found that the paramagnetic maximum principal susceptibility is parallel to [010], the intermediate principal susceptibility parallel to [001], and the minimum susceptibility normal to the (100) plane, and that the AMS ellipsoid has a highly oblate shape. The ferromagnetic contribution or the low-field AMS of the same samples did not show this consistent relationship between magnetic anisotropy and crystal lattice directions. The fact that the macroscopic lineation is defined by the long axis of needle-shaped or prismatic minerals, which does not coincide with the maximum susceptibility direction for amphiboles, calls for a thorough assessment of the link between amphibole CPO and magnetic fabric.

In this study, we examine the magnetic and mineral fabrics of amphibolites from two localities, and predict by model calculations how the magnetic fabric varies for different amphibole textures. The amphibolites from both localities are similar in composition, containing ca. 70 % hornblende, and fabric strength, with hornblende defining the fabric. Still, they display fundamentally different relationships between their maximum susceptibility and lineation, i.e., parallel and oblique. This contribution focuses on how the details of the CPO define the magnetic anisotropy, without intention of interpreting the AMS fabric any further in a structural or regional context. Numerical simulations with model CPOs help predict how different magnetic fabrics can arise for a variety of hornblende textures. Understanding how the type of amphibole texture affects the magnetic fabric is important to facilitate future interpretations of AMS in amphibole-bearing rocks.

2. Material and methods

2.1 Sample description

The samples investigated in this study are from two groups of amphibolites. The first group, which is from a garnet amphibolite in the Ivrea Zone, Northern Italy (GRTA1, GRTA2), has its maximum paramagnetic susceptibility parallel to the macroscopic lineation, whereas the second group from Møre-Trøndelag Fault Complex (Fb3, Fc1) in Central Norway has the maximum susceptibility deviating by up to 50° to mineral lineation (Biedermann, 2010; Biedermann et al., 2015b). All samples contain mainly hornblende, and additionally quartz and plagioclase (Table 1, Figure 1). Quartz and plagioclase are weakly magnetic compared to hornblende. Their presence lowers the rock's mean susceptibility as well as the degree of anisotropy, however, their effect on the orientation of principal susceptibility directions can be neglected. Magnetite occurs as a trace mineral. For this reason, high-field methods were used to separate the paramagnetic hornblende contribution, which is the main interest for this study, from the total magnetic anisotropy. EBSD and magnetic analyses were performed on two core samples from each locality. The EBSD scans were acquired on a surface cut normal to the long axes of the same cores used for magnetic measurements.

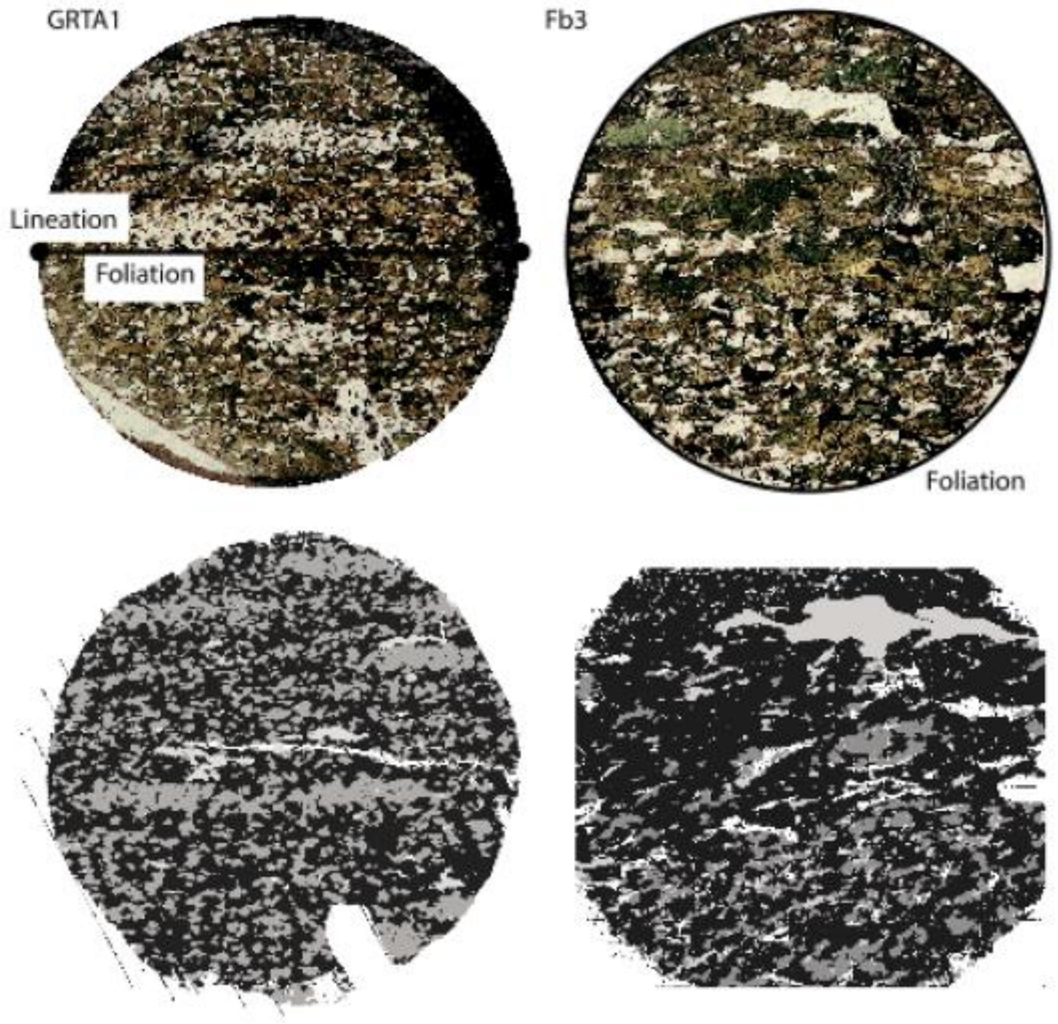

Figure 1: Thin section photographs (above) and EBSD-derived phase maps (below) of GRTA1 and Fb3. Color codes for phase maps: hornblende – black; plagioclase – dark grey; quartz – light grey; not indexed – white. Diameter 1.5 cm for GRTA1, and 2.5 cm for Fb3.

Table 1: Modal composition of each sample (volume percentages, as determined by EBSD)

Sample	Hornblende	Plagioclase	Quartz	Other (<1% unless specified)
GRTA1	67	31	2	Garnet, magnetite
GRTA2	71	27	2	Garnet, magnetite
Fb3	80	12	8	Biotite, epidote, magnetite
Fc1	72	19	5	Pyroxene (3%), biotite, epidote, magnetite

2.2 Mineral fabric

Macroscopic fabrics were observed in the field and in block samples before cores were drilled. They are defined by the preferred alignment of hornblende minerals, as well as the orientation of quartz and plagioclase bands or lenses.

Electron backscatter diffraction (EBSD) on well-polished core surfaces was applied to determine the CPO of amphibole, plagioclase and quartz. Prior to measurements, the sides of each core were covered with silver paint to reduce charging, but no coating was applied to the analyzed surface. EBSD patterns and energy dispersive X-ray spectroscopy (EDS) counts of specific elements were mapped simultaneously with an EOscan Tescan Vega-3 scanning electron microscope (SEM) (Tescan, Brno CZ), equipped with a Pegasus EBSD and EDS system (OIM (Orientation Imaging Microscopy) version 6.2) by Ametek-Edax (Mahway, NJ, USA). The SEM was operated with a beam current of 3-5 nA and 20 kV acceleration voltage. During data acquisition, only one high-symmetry phase was indexed to avoid any loss of speed. All relevant mineral phases were indexed during post-processing using the ChiScan routine of OIM Data Collection, applying user-defined windows for EDS counts to assign the individual minerals. Orientation density functions and pole figures were calculated using the Matlab toolbox MTex (mtex-toolbox.github.io, Hielscher and Schaeben, 2008; Bachmann et al., 2010; Mainprice et al., 2011).

2.3 Magnetic fabric

The magnetic fabric was characterized by the isolated paramagnetic component from high-field AMS measurements on a torque magnetometer (Martín-Hernández and Hirt, 2001). The paramagnetic component was isolated in order to remove any contribution of magnetite to the AMS fabric. Magnetite with its strong susceptibility could dominate the magnetic properties, even though it only contributes < 1% to the rock's composition and may record a different fabric than the major constituents of the rock. Torque measurements were performed in three mutually perpendicular planes, rotating the sample at 30° increments in six fields between 1.0 and 1.5 T on a home-built torsion magnetometer (Bergmüller et al., 1994). Torque can be measured at room temperature or at 77 K, by submersing and measuring the sample in a cryostat filled with liquid nitrogen (Schmidt et al., 2007). At low temperature, the paramagnetic signal is enhanced, because the paramagnetic susceptibility increases with decreasing temperature.

Magnetic susceptibility is described by a second-rank symmetric tensor *k*. Torque measurements are particularly accurate because susceptibility differences are measured instead of absolute values. They define the deviatoric susceptibility tensor, i.e. $\mathrm{k} - \mathrm{k}_{\mathrm{mean}}\mathrm{I}_3$, where I_3 is the 3x3 unit matrix. The eigenvalues of the tensor *k*, $k_1 \geq k_2 \geq k_3$ or $k_1 - k_{mean} \geq k_2 - k_{mean} \geq k_3 - k_{mean}$, are referred to as maximum, intermediate and minimum principal susceptibility, and the corresponding eigenvectors define the direction of each principal susceptibility axis. $\mathrm{k}_{\mathrm{mean}} = \frac{1}{3}(\mathrm{k}_1 + \mathrm{k}_2 + \mathrm{k}_3)$ is the mean susceptibility. Numerous parameters exist to quantify the degree and shape of the anisotropy. In this study, *k'*, describing the deviation of the AMS ellipsoid from a sphere with radius k_{mean}, will be used to describe the anisotropy degree $\mathrm{k}' = \sqrt{[(\mathrm{k}_1 - \mathrm{k}_{\mathrm{mean}})^2 + (\mathrm{k}_2 - \mathrm{k}_{\mathrm{mean}})^2 + (\mathrm{k}_3 - \mathrm{k}_{\mathrm{mean}})^2]/3}$ (Jelinek, 1984), and the shape of the AMS ellipsoid is quantified by $\mathrm{U} = (2\mathrm{k}_2 - \mathrm{k}_1 - \mathrm{k}_3)/(\mathrm{k}_1 - \mathrm{k}_3)$ (Jelinek, 1981). *k'* increases with increasing anisotropy, and *U* varies from -1 for rotationally symmetric prolate ellipsoids to +1 for rotationally symmetric oblate ones; *U* = 0 refers to neutral shape. Note that *k'* is defined for both full and deviatoric tensors, and particularly suited to describe the contribution of a specific component to the whole-rock anisotropy.

2.4 Numerical modelling

The paramagnetic anisotropy in a rock depends on (1) the single crystal magnetic anisotropy of relevant minerals, i.e. amphiboles in this study, (2) the modal composition (volume percentage) of those relevant minerals, and (3) the orientation distribution of the mineral(s) (Fig. 2). Because magnetic susceptibility and AMS are properties of the grain volume, and not the grain boundaries, as for instance in the case of electrical conductivity, it is possible to compute theoretical predictions of the whole-rock AMS based on these three factors (Biedermann et al., 2015b; Mainprice et al., 2011; Mainprice and Humbert, 1994). Other components, such as shape or distribution anisotropy, are important in strongly ferromagnetic minerals, e.g. magnetite, but these do not contribute to the paramagnetic anisotropy. In this study, whole-rock AMS will be characterized by Hill average tensors (Hill, 1952) as computed by MTex. Due to their low mean susceptibility and *k′* (Biedermann et al., 2016; Voigt and Kinoshita, 1907), neither quartz nor plagioclase affect the principal susceptibility directions. Therefore, input parameters for directional models are the single crystal AMS of hornblende, as well as the CPO of amphibole, determined from EBSD data. The mean susceptibility, as well as the values of k_1, k_2 and k_3, and *k′* on the other hand, are influenced the low-susceptibility, low-anisotropy minerals, and thus depend on the modal composition. Because these minerals can have weakly diamagnetic to weakly paramagnetic susceptibilities, their cumulated effect is modeled by adding an isotropic phase with k_{mean} = 1*10^{-9} m^3/kg and given modal percentage to the predicted hornblende susceptibility tensor. Both the orientation of the principal axes, and the degree and shape of the modeled AMS were then compared to the measured paramagnetic AMS.

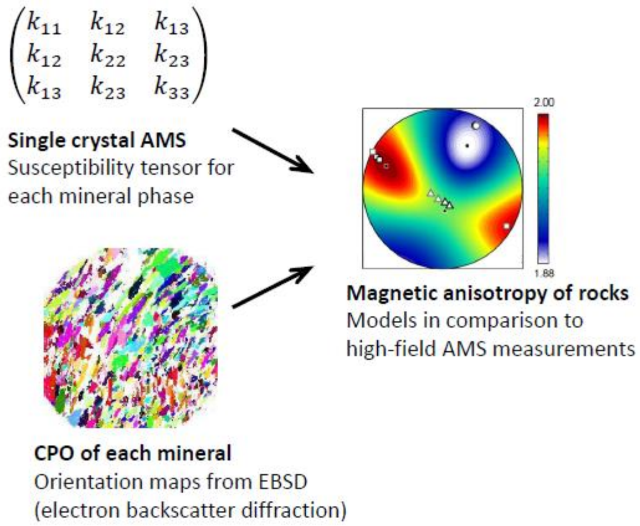

Figure 2: Schematic overview of parameters influencing the magnetic anisotropy in a rock.

An average hornblende tensor was computed from six representative single crystal AMS datasets as reported by Biedermann et al. (2015a). In a first step, full paramagnetic susceptibility tensors were computed from the deviatoric tensor and an independent estimate of mean susceptibility. The latter was determined by (1) low-field measurements, (2) high-field slopes of hysteresis loops, or (3) computations based on the chemical composition. To give each dataset equal weight, all six tensors were then normalized by their mean susceptibility, and an average normalized tensor was calculated. This was multiplied by the average of the mean susceptibilities, resulting in the following magnetic susceptibility tensor for hornblende at room temperature, in a crystal coordinate system with a*= (100) II X, b=[010] II Y, c=[001] II Z (all entries in $10^{-7}\frac{m^3}{kg}$):

$$\underbrace{\begin{pmatrix} 1.779 & 0 & 0 \\ 0 & 2.044 & 0 \\ 0 & 0 & 2.014 \end{pmatrix}}_{\text{full tensor}} = \underbrace{\begin{pmatrix} 1.946 & 0 & 0 \\ 0 & 1.946 & 0 \\ 0 & 0 & 1.946 \end{pmatrix}}_{k_{mean}} + \underbrace{\begin{pmatrix} -0.167 & 0 & 0 \\ 0 & 0.098 & 0 \\ 0 & 0 & 0.068 \end{pmatrix}}_{\text{deviatoric tensor}}$$

3. Results

3.1 Crystallographic preferred orientation (CPO)

The amphibolite samples from both locations show a clear macroscopic fabric, defined by grain shape and compositional banding (Fig. 1). The macroscopic fabrics are characterized by a strong lineation in the Ivrea Zone samples, and a well-defined foliation in combination with a weaker lineation in the samples from the Møre-Trøndelag Fault Zone. The latter is evident by the dispersion of long axes of the hornblende crystals. Fig. 3 shows the pole figures of the (100), [010], and [001] crystallographic poles, respectively, for each sample. Hornblende shows a clear CPO in all samples, with a preferred alignment of [001] axes along the lineation, and of (100) poles normal to the foliation plane. A major difference between the samples is the spread in the distribution of each crystallographic axis: In the garnet amphibolite from the Ivrea Zone, the [001] axes form a point distribution close to the lineation, whereas (100) and [010] spread along a girdle normal to that [001]-maximum. In the amphibolite from the Møre-Trøndelag Fault Zone, on the contrary, the crystallographic (100) direction tends towards a point distribution, and [010] and [001] are more spread along a great circle normal to this direction. These observations agree with the macroscopic fabric, and the maxima of (100) poles and [001] directions are close to the pole to macroscopic foliation, and the macroscopic lineation, respectively.

3.2 Magnetic anisotropy

Table 2 provides an overview of the paramagnetic anisotropy of each sample at room temperature and at 77 K. Principal susceptibility directions are similar at room temperature and 77 K (Fig. 4). All samples have their minimum susceptibility approximately normal to the foliation plane. The orientation of the maximum susceptibility depends on the geologic setting. Both samples from the Ivrea Zone possess a maximum susceptibility sub-parallel to lineation, i.e. an angle of less than 14° between lineation and maximum susceptibility. In contrast, in the samples from the Møre Trøndelag Fault Complex none of the principal susceptibility axes is parallel to the lineation. Both the intermediate and maximum susceptibilities lie approximately in the foliation plane, but there is an angle of 38° - 49° between the maximum susceptibility and lineation. At room temperature, *k'* varies between $9.8 \cdot 10^{-9}$ m^3/kg and $2.2 \cdot 10^{-8}$ m^3/kg, and at 77 K it is higher, ranging from $8.2 \cdot 10^{-8}$ m^3/kg to $1.9 \cdot 10^{-7}$ m^3/kg. All samples have an AMS ellipsoid with oblate shape. *U* varies from 0.47 to 0.64 at room temperature, and 0.46 to 0.68 at 77 K. Comparing *k'* at both temperatures reveals that it increases by a factor of ca. 8-9 upon cooling to 77 K.

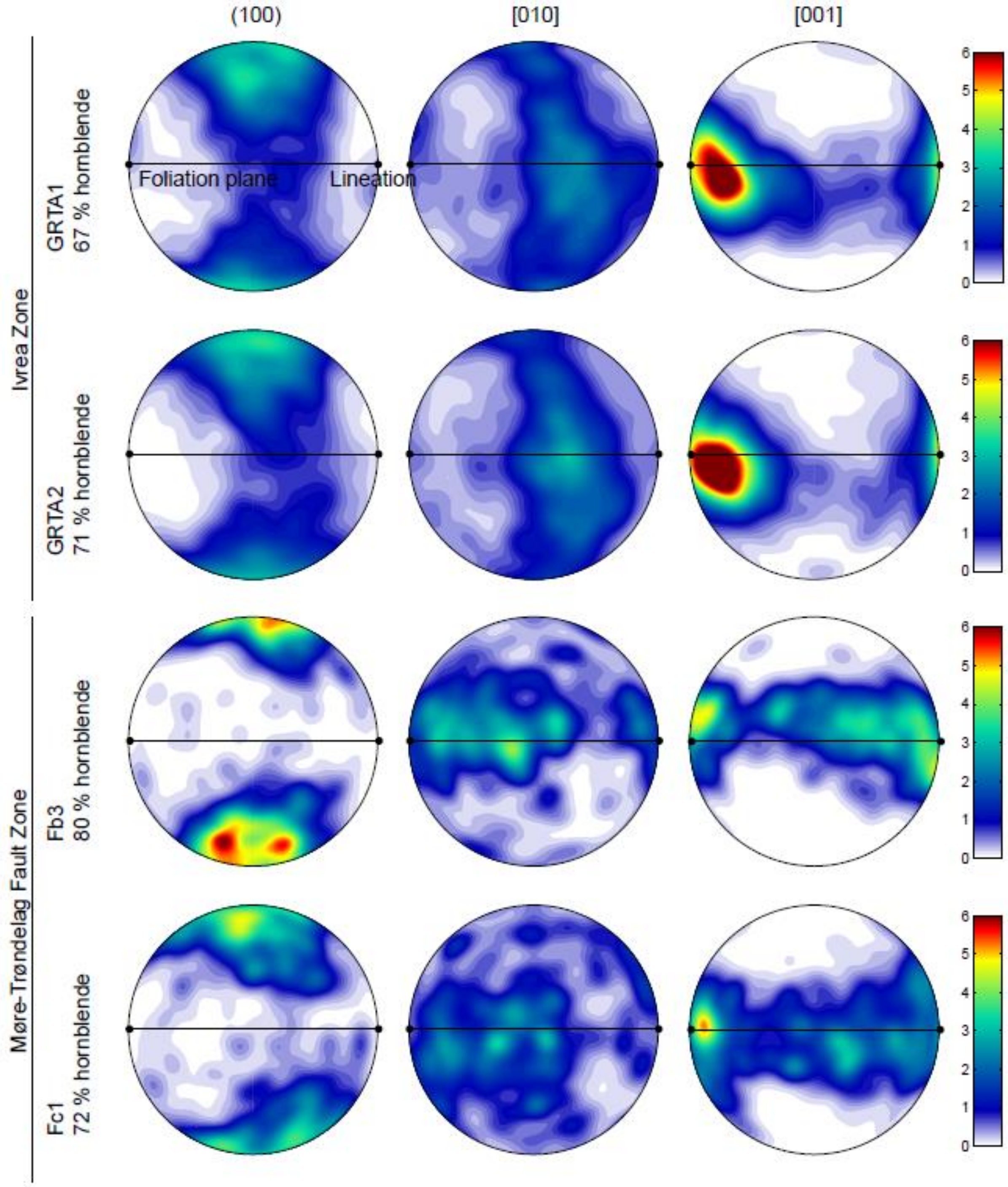

Figure 3: Upper hemisphere stereoplots showing pole figures of three perpendicular crystallographic axes. Equal color scale showing multiples of uniform distribution (m.u.d). Samples are oriented corresponding to their macroscopic foliation and lineation (lineation pointing horizontally, and foliation perpendicular to projection plane).

Table 2: Principal paramagnetic axes, degree and shape of the AMS. Upper hemisphere, foliation-lineation coordinate system: Declination = 0/180, inclination = 0 corresponds to the pole to foliation; declination =90/270, inclination = 0 to the lineations.

Sample	Temperat	% para	k1-kmean	D1	I1	k2-kmean	D2	I2	k3-kmean	D3	I3	U	k'
GRTA1	RT	92 ± 8	9.40E-09	270.1	8.7	4.08E-09	100.0	81.2	-1.35E-08	0.3	1.5	0.54	9.79E-09
GRTA1	77 K	96 ± 4	7.74E-08	91.7	8.3	4.41E-08	269.3	81.7	-1.21E-07	1.7	0.3	0.66	8.67E-08
GRTA2	RT	84 ± 17	1.00E-08	270.2	14.4	3.71E-09	101.0	75.3	-1.37E-08	0.8	2.6	0.47	1.00E-08
GRTA2	77 K	95 ± 41	7.17E-08	271.1	1.1	4.24E-08	148.8	87.9	-1.14E-07	1.2	1.8	0.68	8.15E-08
Fb3	RT	97 ± 16	1.93E-08	277.9	44.7	1.04E-08	65.8	40.6	-2.96E-08	170.7	16.6	0.64	2.13E-08
Fb3	77 K	97 ± 29	1.68E-07	278.7	47.7	9.73E-08	66.4	37.6	-2.65E-07	169.7	16.6	0.67	1.90E-07
Fc1	RT	97 ± 40	1.58E-08	255.1	35.2	6.45E-09	54.9	53.0	-2.23E-08	158.1	9.8	0.51	1.62E-08
Fc1	77 K	96 ± 32	1.49E-07	256.6	36.6	5.34E-08	53.7	51.1	-2.02E-07	158.1	11.3	0.46	1.48E-07

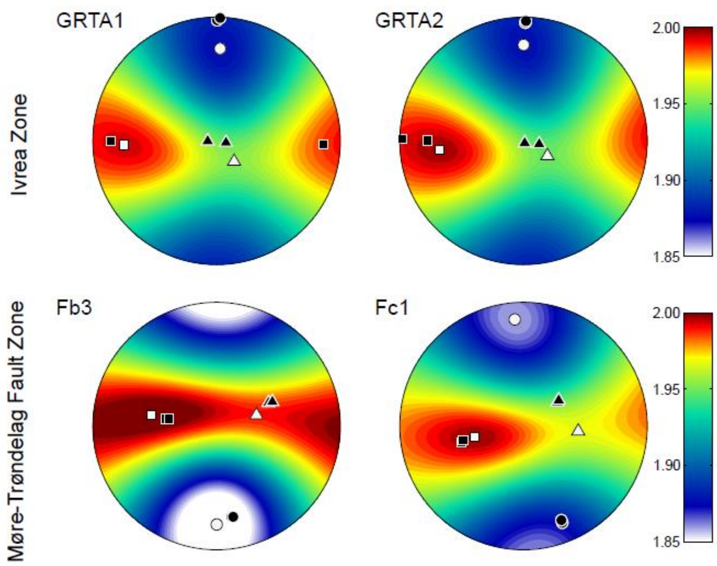

Figure 4: Upper hemisphere stereoplots showing a comparison between the modeled (color coded, in 10^{-7} m^3/kg, white symbols indicate eigenvector directions) and measured paramagnetic AMS (black symbols; square maximum, triangle intermediate and circle minimum susceptibility) at both room temperature and 77 K. Same sample reference as in Fig. 3.

3.3 Modeled magnetic fabric

The AMS ellipsoid modeled from the hornblende texture has principal susceptibility axes that agree well with the orientation of the measured principal axes (Fig. 4). The modeled minimum susceptibility is found to lie approximately normal to the foliation plane. The angle between the modeled and measured minimum susceptibility axes at RT is between 12° and 15° in the samples from the Ivrea Zone, and between 11° and 25° for the Møre Trøndelag Fault Zone amphibolites. For the maximum principal susceptibility, the angle between modeled and measured principal directions is ca 8° for the Ivrea Zone samples and about 11° for the Møre Trøndelag samples. The modeled *k'* shows values between $5*10^{-9}$ m^3/kg and $8*10^{-9}$ m^3/kg (hornblende only), or $3*10^{-9}$ m^3/kg and $6*10^{-9}$ m^3/kg (70 % hornblende, 30 % isotropic phase), which is lower than the measured degree of anisotropy. Modeled AMS shapes are oblate, consistent with measurements, but also show a larger variation between 0.19-0.31 for GRTA samples, and 0.57-0.81 for F samples (Table 3).

Table 3: Parameters of modeled AMS for pure hornblende composition (top) and a mixture of 70 % hornblende (measured CPO) with 30 % plagioclase (uniform CPO, thus effectively isotropic).

	Hornblende only					
Sample	**kmean**	**k1-kmean**	**k2-kmean**	**k3-kmean**	**k'**	**U**
GRTA1	1.94E-07	5.32E-09	1.21E-09	-6.54E-09	4.92E-09	0.31
GRTA2	1.94E-07	5.69E-09	7.57E-10	-6.44E-09	4.98E-09	0.19
Fb3	1.94E-07	6.42E-09	4.78E-09	-1.12E-08	7.95E-09	0.81
Fc1	1.94E-07	5.70E-09	2.65E-09	-8.35E-09	6.03E-09	0.57

	70% hornblende + 30% isotropic phase					
Sample	**kmean**	**k1-kmean**	**k2-kmean**	**k3-kmean**	**k'**	**U**
GRTA1	1.36E-07	3.73E-09	8.49E-10	-4.58E-09	3.44E-09	0.31
GRTA2	1.36E-07	3.98E-09	5.30E-10	-4.51E-09	3.49E-09	0.19
Fb3	1.36E-07	4.50E-09	3.35E-09	-7.85E-09	5.57E-09	0.81
Fc1	1.36E-07	3.99E-09	1.85E-09	-5.85E-09	4.22E-09	0.57

4. Discussion

4.1 Relationship between paramagnetic AMS and amphibole texture

The orientation of the paramagnetic fabric of all four amphibolite samples can be adequately modeled based on the hornblende CPO and an averaged single crystal tensor for hornblende. The modeled *k′* is about a factor of two lower than the measured *k′*. For the samples from the Møre-Trøndelag Fault Complex, other minerals that are present in small amounts (pyroxene, biotite), may add to the measured anisotropy. It should also be noted, however, that the modeled AMS assumes an average hornblende tensor instead of one for the exact composition of the minerals in these rocks. This is important, because the anisotropy parameter *k′* increases with iron content (Biedermann et al., 2015a).

Of particular interest for this study is a comparison of AMS and mineral fabric. The minimum susceptibility axis is approximately normal to the foliation plane in all samples. The maximum susceptibility axis is sub-parallel to the lineation (angular deviation between 1^{o} and 14^{o}) in the amphibolites from the Ivrea Zone. However, in amphibolites from the Møre-Trøndelag Fault Complex, the magnetic and mineral lineations have significantly different orientations, deviating 38^{o} to 49^{o}. Thus, even though: (1) samples from both locations have similar modal compositions; (2) the magnetic fabrics can be well modeled from the hornblende CPO; and (3) the hornblende CPOs follow consistent trends with respect to the mineral fabric defined by foliation and lineation, the principal axes of the AMS ellipsoids and mineral fabrics are co-axial in the Ivrea Zone samples, but not in the Møre-Trøndelag Fault Complex samples. This apparent discrepancy can be explained by the orientation of the maximum susceptibility axis in hornblende single crystals, which is parallel to [010], rather than [001] that defines the lineation. The latter corresponds to the direction of intermediate principal susceptibility in amphibole single crystals. The maximum principal susceptibility, which is parallel to the [010] axis, is only slightly larger than the intermediate susceptibility, whereas the minimum susceptibility, normal to (100), is significantly smaller than both

(Biedermann et al., 2015a). Therefore, if all the amphibole [001]-axes are preferentially aligned with the lineation, the orientation of the magnetic fabric depends on the distribution of the other crystallographic axes. For this reason, it cannot be expected that the maximum susceptibility is always parallel to lineation in rocks whose AMS is dominated by amphiboles. Instead, the rock texture, namely whether the crystallographic axes follow point or girdle distributions, has a major influence (Figure 5).

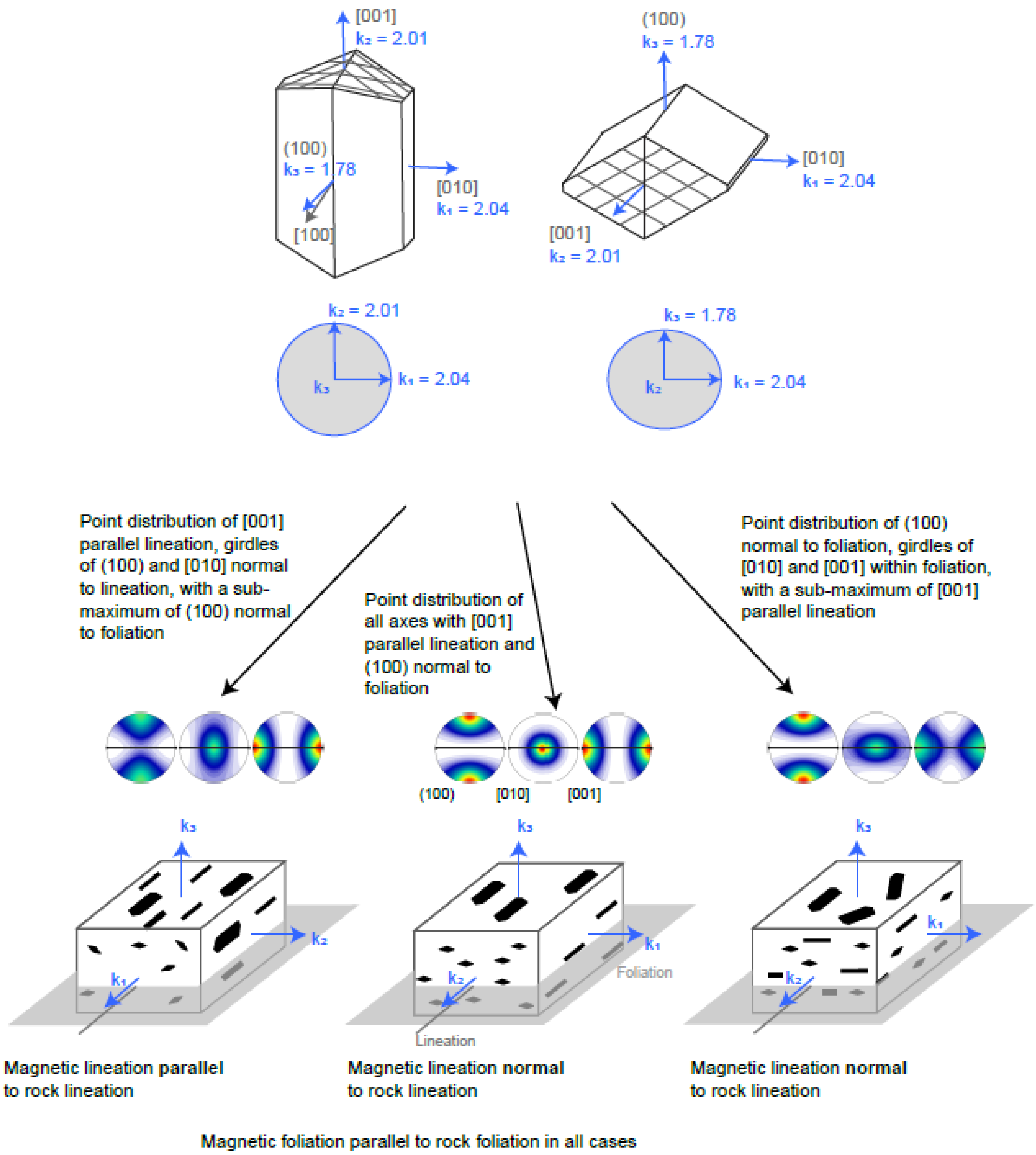

Figure 5: Single crystal magnetic anisotropy in hornblende crystals (data from Biedermann et al., 2015a), and expected magnetic fabrics in rocks of different textures. Susceptibility values given in 10^{-7} m^3/kg. The three model rocks correspond to lineation-dominated (left), strong lineation and strong foliation (middle) and foliation-dominated (right) textures.

4.2 Effects of texture type on magnetic fabrics: Synthetic models

The effect of girdle versus point distributions of the crystallographic axes on magnetic fabrics was further investigated using numerical simulations with model textures. Model textures were created for and between the following three end-members using different shape parameters of the Bingham distribution of quaternions (Kunze and Schaeben, 2005): (1) point distribution of all axes, (2) a-fiber (i.e. point distribution of (100) and girdle distributions of [010] and [001]), and (3) c-fiber texture (i.e. point distribution of [001] and girdle distributions of (100) and [010]). The dispersion of axes in the Bingham distribution, i.e. the degree of alignment, is characterized by the λ parameter, where higher λ indicates stronger concentration. Modeled principal susceptibilities and magnetic fabrics for these textures, with nearly perfect alignment as well as texture strength similar to the samples in this study, are shown in Figure 6. Figure 7 illustrates the variation of AMS principal axes, anisotropy degree *k'* and shape *U* as a function of texture type and texture strength. In addition to the Bingham parameter λ, Figure 7 also shows the corresponding variation of the texture index J (e.g. Bunge 1969, 1982; Mainprice et al., 2015), which is more commonly used to describe the texture strength. Mineral and magnetic lineations are parallel for model textures close to the c-fiber end-member, independent of texture strength. For model textures close to point distribution or between point distribution and a-fiber textures, the magnetic anisotropy possesses oblate shape with the magnetic lineation perpendicular to the fabric lineation, still within the foliation plane. For end-member a-fiber textures, the magnetic lineation is undefined within the foliation plane. The transition between these two situations – k_1 parallel or normal to lineation – becomes closer to the c-fiber endmember for increasing texture strength. It is evident that c-fiber textures create weaker anisotropy than point distributions or a-fiber textures. The anisotropy arising from a point distribution is highest, in the extreme case of perfect crystal alignment reaching that of a single crystal. Because of the oblate shape of hornblende single crystal AMS, the difference in *k'* between point distribution and a-fiber textures is small.

4.3 Implications for using amphibole AMS as fabric indicator

Whereas our model textures represent idealized textures which are symmetric with respect to macroscopic foliation and lineation, rock textures are more complicated and generally possess asymmetries. Because the orientation distributions in rocks are less ideal than in the models, k_1 may also be oblique to the structural lineation rather than perpendicular if a rock's texture is close to point distribution or a-fiber. This indicates that the k_1 direction is not always a reliable proxy for lineation direction in rocks whose AMS is dominantly carried by amphiboles. Namely, maximum susceptibility reliably indicates macroscopic lineation only in rocks displaying c-fiber textures. In rocks with point distributions or a-fiber textures, the direction indicated by maximum susceptibility will be oblique or perpendicular to the macroscopic lineation. Based on this result, and provided that hornblende contributes significantly to the AMS in the hornblende granitic rocks that were investigated by Balsley and Buddington (1960), we would postulate that amphibole in these rocks contains quite some contribution of a c-fiber texture. Interestingly, AMS will correctly indicate lineation directions for a larger range of c-fiber-like textures for weak fabric strengths. Moreover, the strength of magnetic lineation ($L = k_1/k_2$) is not a good indicator of how well amphiboles define the macroscopic lineation. For each texture strength there will be one distinct texture type as combination of c-fiber and point distributions resulting in $k_1 = k_2$, where the magnetic lineation is not defined (i.e., $U = 1$). For stronger textures, $k_1 = k_2$ results for model textures that are more strongly dominated by c-fiber distributions, which relate to lineation-dominated fabrics. Therefore, the shape of the magnetic anisotropy does not unambiguously correlate with texture type: Whereas prolate AMS ellipsoids indicate c-fiber or lineation dominated textures, oblate ellipsoids may correspond to any of the following textures: (1) intermediate between c-fiber and point distribution; (2) point distributions; (3) a-fiber textures; or (4) intermediate between a-fiber and point distribution. The degree of anisotropy generally increases with texture strength for any given texture type. However, it is also strongly affected by texture type, as c-fiber textures display lower degrees of anisotropy than point distributions or a-fiber textures with similar texture strength. The simulations further suggest that if the AMS of a rock is controlled by hornblende, and the maximum susceptibility is parallel to lineation, the rock has predominantly a c-fiber texture. On the other hand, if the maximum susceptibility is normal to lineation and within the foliation plane, any textures between point distributions and a-fiber textures are possible. The transition between these end-members is gradual. This model may explain the 'anomalous' fabrics as reported by Borradaile et al. (1993), as well as the deviation between macroscopic lineation and k_1 described by Biedermann (2010).

Various amphibole fabrics have been observed in nature (Sander, 1930; Schmidt, 1928). Commonly, the long axes of the amphiboles, i.e. [001], define the lineation in a rock, and either <110> axes or (100) poles are perpendicular to the foliation, or the [010] axes form a great circle normal to the lineation (Gapais and Brun, 1981; Mainprice and Nicolas, 1989; Rousell, 1981; Schwerdtner, 1964; Shelley, 1994). Gapais and Brun (1981) measured SPO of grains in amphibolites and found a broad spread in fabrics between planar and linear types. Strong point maxima of [001] axes and girdle distributions of (100) and [010] with sub-maxima, similar to the c-fiber model textures, have been reported by Schwerdtner (1964) in banded hornblende gneiss, and by Rousell (1981) in amphibolite facies massive and gneissic rocks. Two blueschist facies cherts, which were measured by Shelley (1994), display point distributions for [001], and the [010] axes are distributed along a great circle normal to this direction in one sample, and grouped in one point for the other sample, similar to our c-fiber and point distribution models. Diaz Aspiroz et al. (2007) investigated metabasites and show various amphibole textures; two resemble the c-fiber textures, two are point distributions, and 3 samples had a texture similar to the a-fiber texture. They related the different CPOs to differences in deformation mechanisms, which depend on temperature, presence of fluid, or the relative strength of different phases in a rock. Leiss et al. (2002) determined textures of amphibolite and quartz amphibolite and found point distributions in one quartz amphibolite sample, and patterns resembling a-fiber textures in three samples. They explain the different textures with variations in the strain regime. An experimental shear deformation study shows either point distributions of all three axes, or a-fiber-like textures depending on the differential stress and temperature during the experiment (Ko and Jung, 2015). Therefore, all three model texture types, and their magnetic fabrics, are relevant in natural geological materials. Results from these models can thus assist in the geologic or geodynamic interpretation of corresponding amphibole-carried magnetic fabrics.

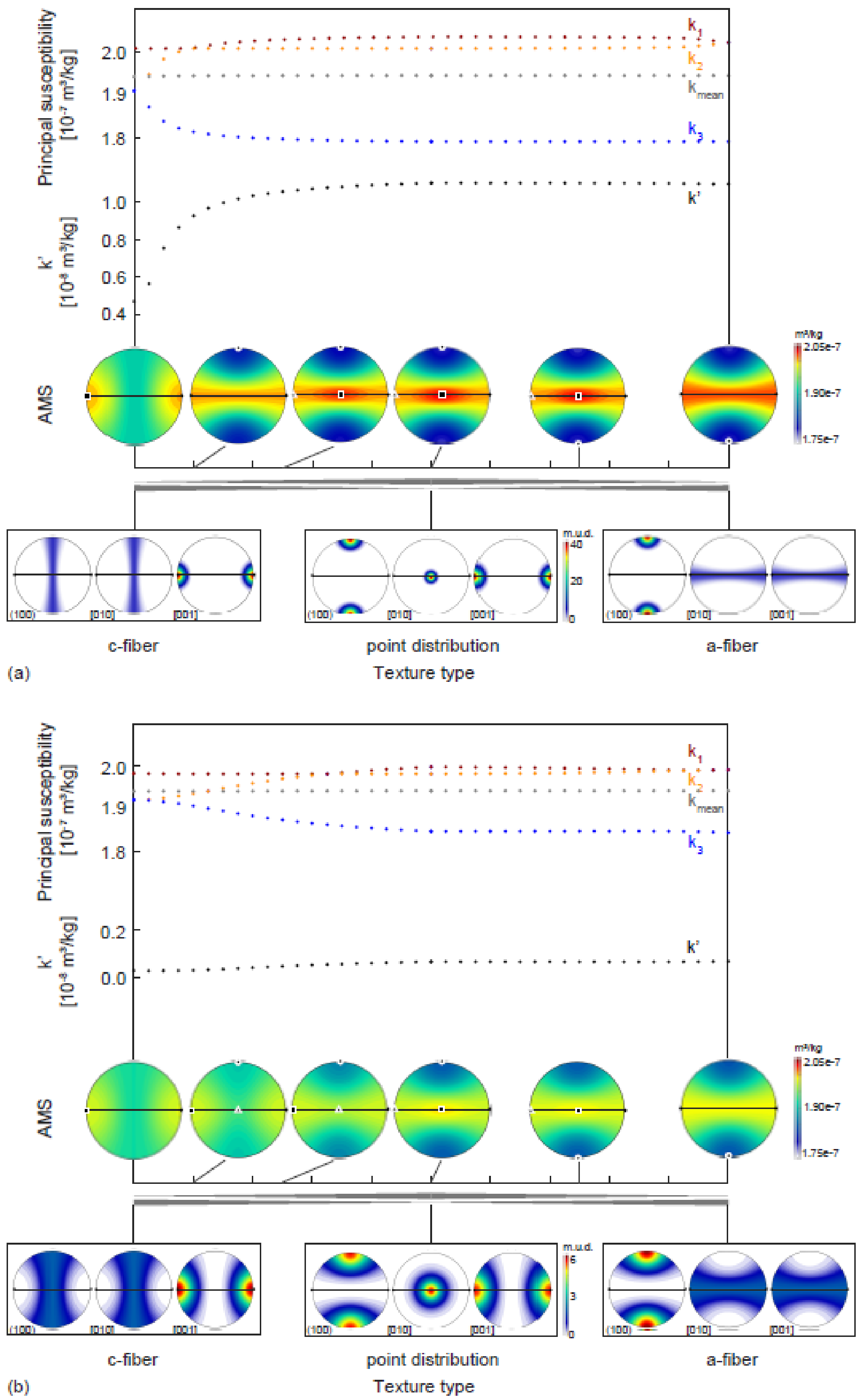

Figure 6: Simulated AMS for a series of model textures of (a) very sharp textures, and (b) texture strengths similar to those encountered in our samples. For both texture strengths, the figures show the variation of principal susceptibilities and k' (top), and magnetic fabrics (middle) in dependence of texture type. End member textures are visualized by sets of three pole figures (bottom), indicating lineation-dominated fiber (left), single component (middle) and foliation-dominated fiber (right) textures. In all model textures, the maximum of the (100) poles is parallel to the foliation pole, and the [001] maximum is parallel to the lineation.

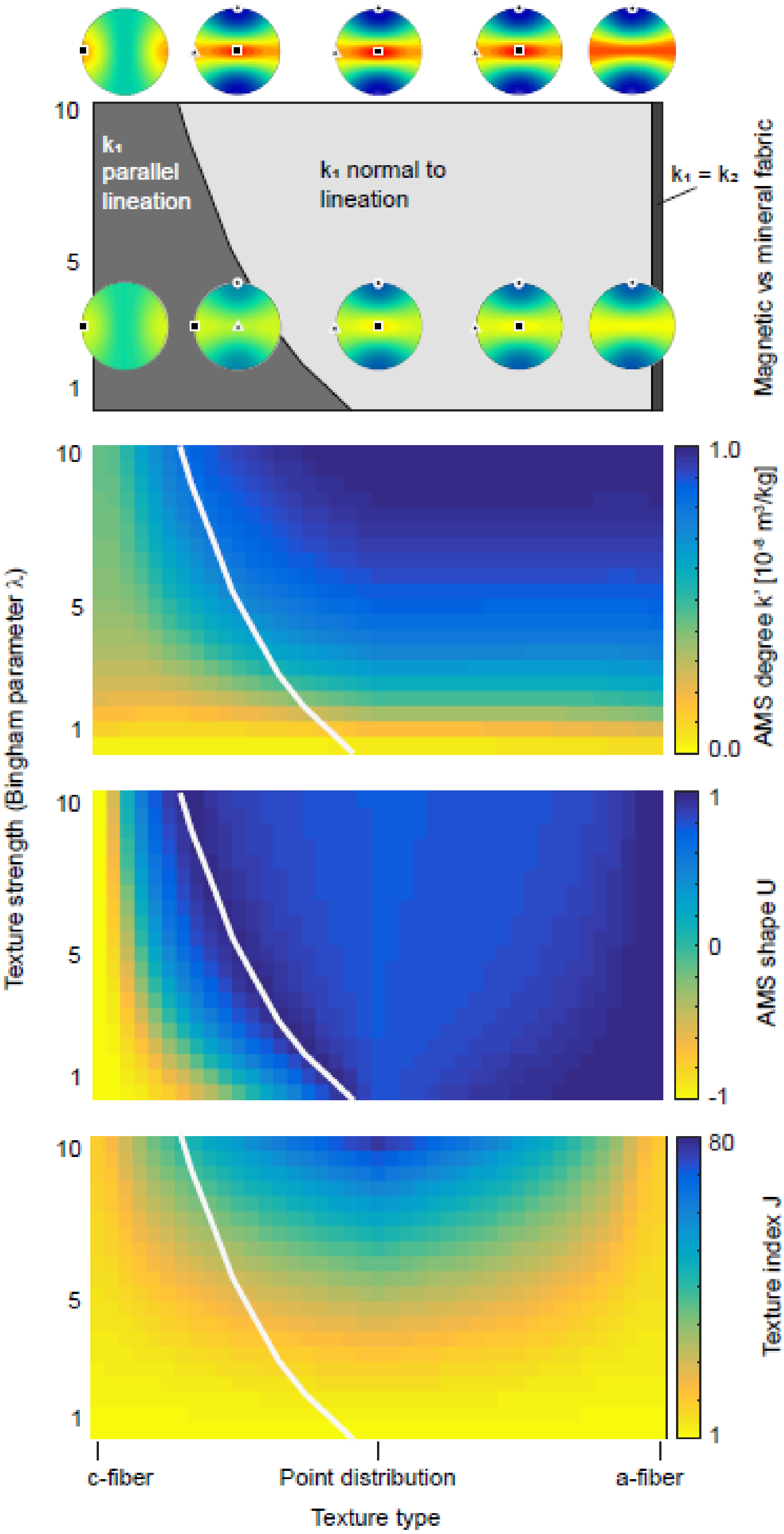

Figure 7: Variation of AMS as a function of texture type and texture strength. Color coded are: Orientation of principal directions (top), AMS degree k' and shape U (center), texture index J (bottom).

5. Conclusion

The relationship between amphibole CPO and the magnetic fabric carried by amphiboles has been investigated based on EBSD-derived CPO data and isolated paramagnetic fabrics in amphibolites, and by numerical simulations of model textures. This study suggests that, similar to CPO-based modeling of seismic or thermal anisotropy, the paramagnetic fabrics in rocks whose AMS is dominated by amphibole can be reliably modeled from single crystal magnetic properties and CPO of hornblende.

Mineral and magnetic fabrics in amphibolites from two locations have been compared. In samples from the Ivrea Zone, which display textures dominated by lineation, the mineral and magnetic lineations are aligned parallel. Samples from the Møre-Trøndelag Fault Complex, whose textures are foliation-dominated, show that the maximum susceptibility axis is tilted far away from the macroscopic lineation direction. Modeling demonstrates that the principal directions of the modeled AMS reflect those of the observed paramagnetic AMS, which is thus correlated to the hornblende texture. Bearing in mind that these models do not provide a direct interpretation of the geodynamic processes leading to the mineral fabric, they allow for a better understanding of the relationship between mineral and magnetic fabric in amphibole-bearing rocks.

Simulated magnetic fabrics from model textures reveal that mineral and magnetic lineations are parallel for the idealized c-fiber end-member textures, but that the magnetic lineation will be perpendicular to the lineation and within the foliation plane for point distributions or a-fiber end-member textures, as well as intermediate textures. Based on these results, it is possible to predict how magnetic and mineral fabrics compare for a variety of texture types and texture strengths, and how the relationship between k_1 and macroscopic lineation may be used for a first estimate of dominant texture type in a sample. Note that rock textures are more complicated than these idealized models. Nevertheless, the models are helpful in explaining observed magnetic fabrics in amphibole-bearing rocks. In particular, the results shown here may explain why so-called 'anomalous' magnetic fabrics, i.e. k_1 not parallel to macroscopic lineation, are observed in some amphibolites, but 'normal' magnetic fabrics in others.

This study shows how model simulations can help in understanding the relationship between magnetic anisotropy and rock texture, and how the orientation of magnetic lineation with respect to the mineral lineation can provide additional information about the mineral fabric. It also explains the conflicting results from earlier studies, and illustrates that understanding the interplay between single crystal anisotropy and mineral texture defining a rock's magnetic fabric is extremely important and prerequisite for any subsequent geodynamic interpretation. This study suggests that combining CPO measurements and numerical simulations based on single crystal properties provides a solid basis for interpreting complex magnetic fabrics.

Acknowledgements

A. Zappone, ETH Zurich, kindly provided the GRTA samples. We are grateful to H.-P. Hächler, ETH Zurich, for preparing sample holders and maintaining the torquemeter. W. Lowrie is thanked for helpful discussions regarding computation of the average single crystal tensors. Access to the SEM EOscan was kindly provided by the Laboratory of Nanometallurgy, ETH Zurich and by ScopeM, through EMEZ project 1154. We are grateful to editor P. Agard, A. Vauchez, C. Cavalcante and an anonymous referee for their detailed reviews. This study was funded by the Swiss National Science Foundation, project 200020_143438.

References

Bachmann, F., Hielscher, R., Schaebenn, H., 2010. Texture Analysis with MTEX - Free and Open Source Software Toolbox. Solid State Phenomena 160, 63-68.

Balsley, J.R., Buddington, A.F., 1960. Magnetic susceptibility anisotropy and fabric of some Adirondack granites and orthogneisses. American Journal of Science 258-A, 6-20.

Bascou, J., Henry, B., Ménot, R.-P., Funaki, M., Barruol, G., 2013. Contribution of AMS measurements in understanding the migmatitic terrains of Pointe Géologie, Terre Adélie (East-Antarctica). Tectonophysics 603, 123-135.

Bascou, J., Raposo, M.I.B., Vauchez, A., Egydio-Silva, M., 2002. Titanohematite lattice-preferred orientation and magnetic anisotropy in high-temperature mylonites. Earth and Planetary Science Letters 198, 77-92.

Bergmüller, F., Bärlocher, C., Geyer, B., Grieder, M., Heller, F., Zweifel, P., 1994. A torque magnetometer for measurements of the high-field anisotropy of rocks and crystals. Meas Sci Technol 5, 1466-1470.

Biedermann, A.R., 2010. Magnetic properties of the Møre Trøndelag Fault Complex. MSc thesis, ETH Zurich, Zurich, Switzerland, DOI: 10.3929/ethz-a-006206930.

Biedermann, A.R., Bender Koch, C., Pettke, T., Hirt, A.M., 2015a. Magnetic anisotropy in natural amphibole crystals. American Mineralogist 100, 1940-1951.

Biedermann, A.R., Kunze, K., Zappone, A.S., Hirt, A.M., 2015b. Origin of magnetic fabrics in ultramafic rocks, IOP Conference Series: Materials Science and Engineering 82(1), DOI:10.1088/1757-899X/82/1/012098

Biedermann, A.R., Pettke, T., Angel, R.J., Hirt, A.M., 2016. Anisotropy of magnetic susceptibility in alkali feldspar and plagioclase. Geophysical Journal International 205, 479-489.

Boiron, T., Bascou, J., Camps, P., Ferré, E.C., Maurice, C., Guy, B., Gerbe, M.-C., Launeau, P., 2013. Internal structure of basalt flows: Insights from magnetic and crystallographic fabrics of the La Palisse volcanics, French Massif Central. Geophysical Journal International 193, 585-602.

Borradaile, G., Keeler, W., Alford, C., Sarvas, P., 1987. Anisotropy of magnetic susceptibility of some metamorphic minerals. Physics of the Earth and Planetary Interiors 48, 161-166.

Borradaile, G.J., Henry, B., 1997. Tectonic applications of magnetic susceptibility and its anisotropy. Earth-Science Reviews 42, 49-93.

Borradaile, G.J., Jackson, M., 2010. Structural geology, petrofabrics and magnetic fabrics (AMS, AARM, AIRM). Journal of Structural Geology 32, 1519-1551.

Borradaile, G.J., Stewart, R.A., Werner, T., 1993. Archean uplift of a subprovince boundary in the Canadian Shield, revealed by magnetic fabrics. Tectonophysics 227, 1-15.

Brownlee, S.J., Hacker, B.R., Harlow, G.E., Seward, G, 2013. Seismic signatures of a hydrated mantle wedge from antigorite crystal-preferred orientation (CPO). Earth and Planetary Science Letters 375, 395-407.

Brownlee, S.J., Hacker, B.R., Salisbury, M., Seward, G. Little, T.A., Baldwin, S.L., Abers, G.A., 2011. Predicted velocity and density structure of the exhuming Papua New Guinea ultrahigh-pressure terrane. Journal of Geophysical Research 116, B08206.

Bunge, H.-J., 1969. Mathematische Methoden der Texturanalyse. Akademie-Verlag, Berlin, Germany.

Bunge, H.-J., 1982. Texture Analysis in Materials Science: Mathematical Models. Butterworths, London, UK.

Cavalcante, G.C.G., Egydio-Silva, M., Vauchez, A., Camps, P., 2013. Strain distribution across a partially molten middle crust: Insights from the AMS mapping of the Carlos Chagas Anatexite, Araçuaí belt (East Brazil). Journal of Structural Geology 55, 79-100.

Chadima, M., Cajz, V., Tycova, P., 2009. On the interpretation of normal and inverse magnetic fabric in dikes: Examples from the Eger Graben, NW Bohemian Massif. Tectonophysics 466, 47-63.

Chadima, M., Hansen, A., Hirt, A.M., Hrouda, F., Siemens, H., 2004. Phyllosilicate preferred orientation as a control of magnetic fabric: Evidence from neutron texture goniometry and low and high-field magnetic anisotropy (SE Rhenohercynian Zone of Bohemian Massif), in: Martín-Hernández, F., Lüneburg, C.M., Aubourg, C., Jackson, M. (Eds.), Magnetic Fabric: Methods and Applications. The Geological Society, London UK, pp. 361-380.

Cogné, J.P., Perroud, H., 1988. Anisotropy of magnetic susceptibility as a strain gauge in the Flamanville granite, NW France. Physics of the Earth and Planetary Interiors 51, 264-270.

Craddock, J.P., McKiernan, A.W., 2007. Tectonic implications of finite strain variations in Baraboo-interval quartzites (ca. 1700 Ma), Mazatzal orogen, Wisconsin and Minnesota, USA. Precambrian Research 156, 175-194.

Diaz Aspiroz, M., Lloyd, G.E., Fernandez, C., 2007. Development of lattice preferred orientation in clinoamphiboles deformed under low-pressure metamorphic conditions. A SEM/EBSD study of metabasites from the Aracena metamorphic belt (SW Spain). Journal of Structural Geology 29, 629-645.

Engler, O. Randle, V., 2009. Introduction to Texture Analysis: Macrotexture, Microtexture, and Orientation Mapping. CRC Press, Boca Raton, US.

Feinberg, J.M., Wenk, H.-R., Scott, G.R., Renne, P.R., 2006. Preferred orientation and anisotropy of seismic and magnetic properties in gabbronorites from the Bushveld layered intrusion. Tectonophysics 420, 345-356.

Finke, W., 1909. Magnetische Messungen an Platinmetallen und monoklinen Kristallen, insbesondere der Eisen-, Kobalt- und Nickelsalze. Annalen der Physik 336, 149-168.

Gapais, D., Brun, J.-P., 1981. A comparison of mineral grain fabrics and finite strain in amphibolites from eastern Finland. Canadian Journal of Earth Sciences 18, 995-1003.

Gaudreau, E., Schneider, D., Lagroix, F., Cossette, E., Grasemann B., 2017, Controls and implications of anisotropy across a strain gradient within granodiorite, Serifos, Greece. Journal of Geodynamics 105, 11-26.

Graham, J.W., 1966. Significance of magnetic anisotropy in Appalachian sedimentary rocks, in: Steinhart, J.S., Smith, T.J. (Eds.), The Earth Beneath the Continents: A Volume of Geophysical Studies in Honor of Merle A. Tuve. American Geophysical Union, Washington, US, pp. 627-648.

Hielscher, R., Schaeben, H., 2008. A novel pole figure inversion method: specification of the MTex algorithm. Journal of Applied Crystallography 41, 1024-1037.

Hill, R., 1952. The elastic behaviour of a crystalline aggregate. Proceedings of the Physical Society A 65, 349-354.

Hirt, A.M., Lowrie, W., Clendenen, W.S., Kligfield, R., 1988. The correlation of magnetic anisotropy with strain in the Chelmsford Formation of the Sudbury Basin, Ontario. Tectonophysics 145, 177-189.

Hrouda, F., 1982. Magnetic anisotropy of rocks and its application in geology and geophysics. Geophysical Surveys 5, 37-82.

Hrouda, F., Schulmann, K., 1990. Conversion of the magnetic susceptibility tensor into the orientation tensor in some rocks. Physics of the Earth and Planetary Interiors 63, 71-77.

Hrouda, F., Schulmann, K., Suppes, M., Ullemeyer, K., de Wall, H., Weber, K., 1997. Quantitative relationship between low-field AMS and phyllosilicate fabric: A review. Physics and Chemistry of the Earth 22, 153-156.

Hrouda, F., Siemes, H., Herres, N., Hennig-Michaeli, C., 1985. The relation between the magnetic anisotropy and the c-axis fabric in a massive hematite ore. Journal of Geophysics – Zeitschrift fur Geophysik 56, 174-182.

Jelinek, V., 1981. Characterization of the magnetic fabric of rocks. Tectonophysics 79, T63-T67.

Jelinek, V., 1984. On a mixed quadratic invariant of the magnetic susceptibility tensor. Journal of Geophysics - Zeitschrift Fur Geophysik 56, 58-60.

Ji, S., Mainprice D., 1989. Seismic anisotropy in the lower crust induced by lattice preferred orientations of minerals. Seismology and Geology 11, 10-24.

Kligfield, R., Lowrie, W., Dalziel, W.D., 1977. Magnetic susceptibility anisotropy as a strain indicator in the Sudbury Basin, Ontario. Tectonophysics 40, 287-308.

Kligfield, R., Lowrie, W., Hirt, A., Siddans, A.W.B., 1983. Effect of progressive deformation on remanent magnetization of Permian redbeds from the Alpes Maritimes (France). Tectonophysics 97, 59-85.

Kneen, S.J., 1976. The relationship between the magnetic and strain fabrics of some haematite-bearing slates. Earth and Planetary Science Letters 31, 413-416.

Ko, B., Jung, H., 2015. Crystal preferred orientation of an amphibole experimentally deformed by simple shear. Nature Communications, 6, 6586. DOI:10.1038/ncomms7586.

Kruckenberg, S.C., Ferré, E.C., Teyssier, C., Vanderhaeghe, O., Whitney, D.L., Seaton, N.C.A., Skord, J.A., 2010. Viscoplastic flow in migmatites deduced from fabric anisotropy: An example from the Naxos dome, Greece. Journal of Geophysical Research 115, B09401.

Kunze, K., Schaeben, H.,, 2005. The Bingham Distribution of Quaternions and Its Spherical Radon Transform in Texture Analysis. Mathematical Geology 36, 917-943.

Lagroix, F., Borradaile, G.J., 2000. Magnetic fabric interpretation complicated by inclusions in mafic silicates. Tectonophysics 325, 207-225.

Leiss, B., Gröger, H.R., Ullemeyer, K., Lebit, H., 2002. Textures and microstructures of naturally deformed amphibolites from the northern Cascades, NW USA: methodology and regional aspects, in: de Meer, S., Drury, M.R., de Bresser, J.H.P., Pennock, G.M. (Eds.), Deformation Mechanisms, Rheology and Tectonics: Current Status and Future Perspectives. Geological Society Special Publications London, UK, pp. 219-238.

Lloyd, G.E., Halliday, J.M., Butler, R.W.H., Casey, M., Kendell, J.M. Wookey, J. Mainprice, D., 2011. From crystal to crustal: petrofabric derived seismic modelling of regional tectonics. In: Prior, D.J., Tutter, E.H., Tatham, D.J. (eds) Deformation Mechanisms, Rheology and Tectonics> Microstructures, Mechanics and Anisotropy. Geological Society London Special Publications 360, 49-78.

Lüneburg, C.M., Lampert, S.A., Lebit, H.D., Hirt, A.M., Casey, M., Lowrie, W., 1999. Magnetic anisotropy, rock fabrics and finite strain in deformed sediments of SW Sardinia (Italy). Tectonophysics 307, 51-74.

Mainprice, D., 1990. An efficient FORTRAN program to calculate seismic anisotropy from the lattice preferred orientation of minerals. Computers and Geosciences 16, 385-393.

Mainprice, D., Bachmann, F., Hielscher, R., Schaeben, H., 2015. Descriptive tools for the analysis of texture projects with large datasets using Mtex: strength, symmetry and components. In: Faulkner, D.R., Mariani, E., Mecklenburgh, J. (eds.) Fock Deformation from Field, Experiments, and Theory: A Volume in Honour of Ernie Rutter. Geological Society, London, Special Publications 409, 251-271.

Mainprice, D., Hielscher, R., Schaeben, H., 2011. Calculating anisotropic physical properties from texture data using the MTEX open-source package. Geological Society, London, Special Publications 360, 175-192.

Mainprice, D., Humbert, M., 1994. Methods of calculating petrophysical properties from lattice preferred orientation data. Surveys in Geophysics 15, 575-592.

Mainprice, D., Nicolas, A., 1989. Development of shape and lattice preferred orientations: application to the seismic anisotropy of the lower crust. Journal of Structural Geology 11, 175-189.

Martín-Hernández, F., Ferré, E.C., 2007. Separation of paramagnetic and ferrimagnetic anisotropies: A review. Journal of Geophysical Research-Solid Earth 112.

Martín-Hernández, F., Hirt, A.M., 2001. Separation of ferrimagnetic and paramagnetic anisotropies using a high-field torsion magnetometer. Tectonophysics 337, 209-221.

Martín-Hernández, F., Lüneburg, C.M., Aubourg, C., Jackson, M., 2004. Magnetic Fabrics: Methods and Applications. The Geological Society, London, UK.

Oliva-Urcia, B., Casas, A.M., Ramón, M.J., Leiss, B., Mariani, E., Román-Berdiel, T., 2012. On the reliability of AMS in ilmenite-type granites: An insight from the Marimanha pluton, central Pyrenees. Geophysical Journal International 189, 187-203.
Owens, W.H., 1974. Mathematical model studies on factors affecting the magnetic anisotropy of deformed rocks. Tectonophysics 24, 115-131.
Owens, W.H., Bamford, D., 1976. Magnetic, seismic, and other anisotropic properties of rock fabrics. Philosophical Transactions of the Royal Society A 283, 55-68.
Owens, W.H., Rutter, E.H., 1978. The development of magnetic susceptibility anisotropy through crystallographic preferred orientation in a calcite rock. Physics of the Earth and Planetary Interiors 16, 215-222.
Parry, G.R., 1971. The magnetic anisotropy of some deformed rocks. University of Birmingham, Birmingham, UK, p. 218.
Punturo, R., Mamtani, M.A., Fazio, E., Occhipinti, R., Renjith, A.R., Cirrincione, R., 2017. Seismic and magnetic susceptibility anisotropy of middle-lower continental crust: Insights for their potential relationship from a study of intrusive rocks from the Serre Massif (Calabria, southern Italy). Tectonophysics 712-713, 542-556.
Rathore, J.S., 1979. Magnetic susceptibility anisotropy in the Cambrian slate belt of North Wales and correlation with strain. Tectonophysics 53, 83-97.
Rousell, D.H., 1981. Fabric and origin of gneissic layers in anorthositic rocks of the St. Charles sill, Ontario. Canadian Journal of Earth Sciences 18, 1681-1693.
Sander, B., 1930. Gefügekunde der Gesteine. Springer, Wien, Austria.
Schmidt, V., Hirt, A.M., Rosselli, P., Martín-Hernández, F., 2007. Separation of diamagnetic and paramagnetic anisotropy by high-field, low-temperature torque measurements. Geophysical Journal International 168, 40-47.
Schmidt, W., 1928. Zur Regelung zweiachsiger Mineralien in kristallinen Schiefern, Neues Jahrbuch der Mineralogie, Geologie und Paläontologie, . E. Schweizerbart'sche Verlagshandlung (Erwin Nägele), Stuttgart, Germany, pp. 203-222.
Schulmann, K., Ježek, J., 2011. Some remarks on fabric overprints and constrictional AMS fabrics in igneous rocks. International Journal of Earth Sciences 101, 705-714.
Schwerdtner, W.M., 1964. Preferred orientation of hornblende in a banded hornblende gneiss. American Journal of Science 262, 1212-1229.
Seront, B., Mainprice, D., Christensen, N.I., 1993. A determination of the 3-dimensional seismic properties of anorthosite - comparision between values calculated from the petrofabric and direct laboratory measurements. Journal of Geophysical Research 98, 2209-2221.
Shelley, D., 1994. Spider texture and amphibole preferred orientations. Journal of Structural Geology 16, 709-717.
Siegesmund, S., Ullemeyer, K., Dahms, M., 1995. Control of magnetic rock fabrics by mica preferred orientation - a quantitative approach. Journal of Structural Geology 17, 1601-1613.
Tarling, D.H., Hrouda, F., 1993. The Magnetic Anisotropy of Rocks. Chapman and Hall, London, UK.
Tommasi, A., Gibert, B., Seipold, U, Mainprice, D., 2001. Anisotropy of thermal diffusivity in the upper mantle. Nature 411, 783-786.
Ullemeyer, K., Braun, G., Dahms, M., Kruhl, J.H., Olesen, N.Ø., Siegesmund, S., 2000. Texture analysis of a muscovite-bearing quartzite: A comparison of some currently used techniques. Journal of Structural Geology 22, 1541-1557.
Viegas, L.G.F., Archanjo, C.J., Vauchez, A., 2013. Fabrics of migmatites and the relationships between partial melting and deformation in high-grade transpressional shear zones: The Espinho Branco anatexite (Borborema Province, NE Brazil). Journal of Structural Geology 48, 45-56.
Voigt, W., Kinoshita, S., 1907. Bestimmung absoluter Werte von Magnetisierungszahlen, insbesondere für Kristalle. Annalen der Physik 329, 492-514.
Wagner, J.-J., Hedley, I.G., Steen, D., Tinkler, C., Vuagnat, M., 1981. Magnetic anisotropy and fabric of some progressively deformed ophiolitic gabbros. Journal of Geophysical Research 86, 307-315.

Wenk, H.-R., Matthies, S., Donovan, J., Chateigner, D., 1998. BEARTEX: a Windows-based program system for quantitative texture analysis. Journal of Applied Crystallography 31, 262-269.

Wood, D.S., Oertel, G., Singh, J., Bennett, H.F., 1976. Strain and anisotropy in rocks. Philosophical Transactions of the Royal Society A 283, 27-42.

Zak, J., Verner, K., Tycova, P., 2008. Multiple magmatic fabrics in plutons: an overlooked tool for exploring interactions between magmatic processes and regional deformation? Geological Magazine 145, 537-551.